Vibrational Spectra and Structure of Kaolinite: A Computer Simulation Study

Daniel Bougeard,*,† Konstantin S. Smirnov,‡ and Ekkehard Geidel§

Laboratoire de Spectrochimie Infrarouge et Raman du CNRS, Université des Sciences et Technologies de Lille, 59655 Villeneuve d'Ascq Cedex, France, Laboratory for Applied Organic Chemistry and Catalysis, Delft University of Technology, Julianalaan 136, 2628 BL Delft, The Netherlands, and Institut für Physikalische Chemie, Universität Hamburg, Bundesstrasse 45, 20146 Hamburg, Germany

Received: April 6, 2000; In Final Form: June 7, 2000

The structure and vibrational spectra of kaolinite have been investigated by the joint use of vibrational spectroscopic techniques and of computational methods. The derived potential is based on ab initio calculations of molecular models and tested in normal mode analyses and molecular dynamics simulations. The calculated structural parameters and vibrational spectra are in a good agreement with experimental data. Taking into account the sensitivity of Raman spectra in the lattice region to the structural characteristics, the spectra were examined in more detail, using different models to compute the polarizability tensor of the system. A complete assignment of the bands observed in the experimental spectra is suggested on the basis of the calculated infrared, Raman and power spectra.

1. Introduction

Since Pauling[1] first obtained information about the crystal structure of kaolinite seventy years ago, kaolin minerals (kaolinite, halloysite, dickite, and nacrite) and their derivatives obtained by intercalation of various species have been objects of intensive experimental and theoretical research. Apart from diffraction techniques and high-resolution solid-state NMR, methods of vibrational spectroscopy are most frequently applied to characterize clay minerals. Infrared (IR) and Raman spectroscopies provide information at the molecular level about the structure and dynamics in a system but for the interpretation of the experimental data a reliable assignment of observed vibrational transitions to normal modes of a given structure is necessary. Already in the case of medium-sized molecules such an assignment, done on purely empirical basis, leads to substantial uncertainties. The interpretation of the spectra of complex compounds, like clays, is even more difficult and thus necessitates the use of computational methods to remove eventual ambiguities from the interpretation. Force field based methods and quantum mechanical techniques yield a detailed description of the systems at the microscopic level and allow a quantitative interpretation of the experimental data. Modeling clay minerals is also of significant interest since clays play an important role in transport processes of natural as well as contaminant species in soils and sediments.

Kaolinite is a layered aluminosilicate with a 1:1 uncharged dioctahedral layered structure.[2−5] Each layer consists of a sheet of SiO_4 tetrahedra forming six-membered silicate rings connected via common oxygen atoms to a sheet of AlO_6 octahedra building four-membered aluminate rings. The kaolinite structure, which is shown in Figure 1, contains two types of hydroxyl groups. The first one is bound to the hexacoordinated aluminum atoms and covers one of the two basal surfaces of the layer; these hydroxyls are therefore called outer hydroxyl groups. The second type of OH groups is situated within the shared plane of the octahedral/tetrahedral sheets (so-called internal or inner hydroxyl groups).

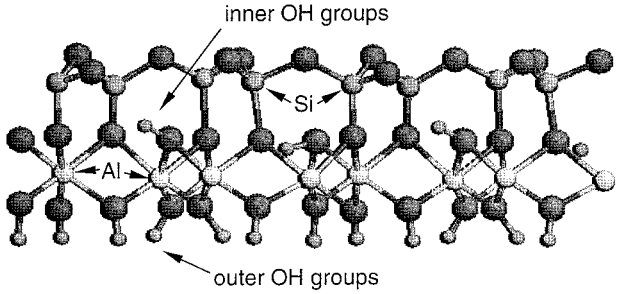

Figure 1. Representation of the structure of a kaolinite sheet built up from 3 × 2 × 1 unit cells.

The vibrational spectra of kaolinite have intensively been studied. IR and Raman spectroscopies were employed to characterize different kinds of OH groups in the hydroxyl stretching frequency range[6−9] as well as in the range of the OH bending modes.[10,11] The studies often included complete[10] or selective deuteration[12,13] of the minerals in order to confirm the suggested assignments of different bands to vibrations of individual types of OH groups. Investigations in the mid- and low-frequency region have been undertaken in order to distinguish between different kaolinite polymorphs[14] (particularly using FT-Raman spectroscopy) or focusing on the observation of changes in the vibrational spectra induced upon intercalation of guest species.[15−17]

The experimental works were complemented by modeling studies dealing with the intercalation processes of a variety of molecules to determine the preferred adsorption sites and the structural characteristics of their local surrounding and/or to get information about the diffusion behavior of the intercalates. So far, in most modeling studies only the interlayer distances were allowed to vary, whereas the layers were treated as rigid. Teppen et al.[18] recently developed an empirical force field model for aluminous clay minerals. The key problem in obtaining the force field parameters lies in the treatment of the octahedral sheet

† Université des Sciences et Technologies de Lille. Fax: +33 3 20436755. E-mail: Daniel.Bougeard@univ-lille1.fr.
‡ Delft University of Technology.
§ Universität Hamburg.

10.1021/jp0013255 CCC: $19.00
Published on Web 09/08/2000

because the 6-fold coordination of aluminum atoms by oxygen in this sheet results in O−Al−O angles near 90° and 180°. This bonding situation is not easily handled by conventional molecular mechanics force fields. The authors performed quantum mechanical ab initio calculations of small molecules,[19] which mimic the 6-fold coordinated Al atoms in clay minerals, and results of those calculations were used to derive the necessary force field parameters. The resulting force field was able to reproduce the major structural features of the clay minerals in agreement with experimental observations. No application of this force field to the calculation of the vibrational spectra of clays was reported in the literature to our best knowledge. However, in molecular dynamics studies (MD) of aluminosilicates[20] it was shown that the dynamical behavior of such lattices is much more sensitive to the potential model than structural characteristics and that the vibrational spectra can successfully be used as supplementary experimental data to evaluate the quality of model potentials.

The purpose of this paper is to develop a force field that is able to predict both the dynamical behavior and the structural characteristics of clays. Force field parameters were obtained on the basis of ab initio calculations of small molecular models representing the octahedral sites in the kaolinite lattice. The obtained force constants were added to a force field for tetrahedrally coordinated aluminosilicates that was recently developed for zeolites following the same strategy.[21−23] The complete force field was then tested in MD simulations and normal-mode analyses (NMA) of kaolinite, and the results of these calculations were used to improve the assignment of the bands observed in the vibrational spectra of kaolinite samples.

2. Experimental and Computational Methodologies

2.1. Experimental Details. The kaolinite samples (kaolinor and granulite) examined were obtained from Kaolins d'Arvor (Ploemoeur, Brittany) and studied without further purification. The provider states that granulite is the pure geological ore including 70% quartz and 15% mica, whereas kaolinor is the enriched product after purification containing at least 80% kaolinite. The infrared spectra of the samples were recorded at room temperature using KBr technique by an FT-IR Bruker spectrometer IFS 88 in the 5000−400 cm^{-1} range with a spectral resolution of 4.0 cm^{-1}. The spectra were averaged over 300 scans.

The Raman spectra were obtained by using a LABRAM Raman spectrometer manufactured by Instruments SA Dilor. The Raman scattering of the samples was excited using the 632.8 nm line of a helium−neon laser. The laser beam was focused through a high-aperture microscope objective and the scattered light collected through the same objective. The sensitive multichannel detection system permitted the use of very low laser power at the sample, typically less than 5 mW. This laser power is low enough to prevent any changes in the structure during the measurement.

2.2. Computational Methods. In vibrational spectroscopy of dense silicates[10] and sheet silicates[24] a usual approximation, analogous to the characteristic group frequency approach for polyatomic molecules, is to assume that the vibrations of a structure can be described in terms of vibrations of its primary building units. This concept has been successfully transferred for the development of force fields for dense and microporous silicates and aluminosilicates.[21−23,25,26] Following this approach, a representative building unit is cut out of a structure and is treated in ab initio calculations as a molecule. The results of the calculation yield parameters of the force field, which is then used in modeling of larger systems. In the case of kaolinite such primary building units are SiO_4 tetrahedra and AlO_6 octahedra connected via common oxygen atoms or Brønsted acidic OH groups.

The force field examined in the present work is a harmonic valence force field defined in terms of internal coordinates. In the model used the potential energy (V) of the system is written as

$$2V = \sum_i K_{ii}^r (r_i - r_i^0)^2 + \sum_k K_{kk}^\alpha (\alpha_k - \alpha_k^0)^2 + \sum_m \frac{K_{mm}^\beta}{\sin^2 \beta_0} (\cos \beta_m - \cos \beta_m^0)^2 + \sum_{i \neq j} k_{ij}^{rr} (r_i - r_i^0)(r_j - r_j^0) + \sum_{k \neq l} k_{kl}^{\alpha\alpha} (\alpha_k - \alpha_k^0)(\alpha_l - \alpha_l^0) + \sum_{m \neq n} k_{mn}^{\beta\beta} (\beta_m - \beta_m^0) \times (\beta_n - \beta_n^0) + \sum_{i \neq k} k_{ik}^{r\alpha} (r_i - r_i^0)(\alpha_k - \alpha_k^0) + \sum_{i \neq m} k_{im}^{r\beta} (r_i - r_i^0)(\beta_m - \beta_m^0) \quad (1)$$

where the first term represents the contribution of bond stretching internal coordinates (r) to the potential energy. The second term stands for the contribution of deformations of the OTO, TOH and TO(H)T out-of-plane angles (α), T means an Si or Al atom. The third term represents the potential energy of TOT angle bendings (β). It should be noted that a cosine harmonic angle bending potential was applied for TOT angles to allow for their high flexibility. The following terms account for the interactions between the internal coordinates. The "0" superscript denotes an equilibrium value of a coordinate.

Force field parameters for the SiO_4 unit and bridging OH groups have already been obtained in our previous studies on siliceous zeolites[21] and aluminosilicates,[22] and thus, only terms for aluminum atoms in octahedral coordination have to be added to the force field. For this purpose the matrix of the second derivatives of the total energy with respect to the Cartesian coordinates ($\mathbf{F}_X$) was calculated using the Gaussian94 program package[27] for the $Al(OH)_6^{3-}$ model, in which the hydrogen atoms were added in order to achieve the bivalence of the oxygen atoms. The preliminary calculations were performed using the 3-21 G* basis set at the Hartree−Fock (HF) level. Since the development of an accurate force field for minerals requires ab initio calculations with larger basis sets and the inclusion of electron correlation,[28] the final calculations were performed employing the 6-311G** basis set at both HF and MP2 levels. The $\mathbf{F}_X$ matrix obtained was then transformed into the matrix of second derivatives in internal coordinates ($\mathbf{F}_R$) using the program REDONG,[29] so that the redundancies existing between the internal coordinates were taken into account. In the set of internal coordinates used for the AlO_6 units, all bond stretching coordinates and all 90° O−Al−O angle bending coordinates were explicitly considered, while the redundant linear O−Al−O angle bending coordinates were excluded.

To examine also kinematic coupling effects in the kaolinite subunits, normal-mode analyses (NMA) were performed for a simple AlO_6 model and for the crystallographic unit cell using the NMA packages for molecules[30] and for crystal lattices,[31] respectively. In these calculations the influence of all force constants k_h of the force field on the vibrational frequencies ν_i was inspected via the elements of the Jacobian matrix J_{ih}

$$J_{ih} = \frac{\delta \upsilon_i}{\delta k_h} \quad (2)$$

Finally, the ability of this force field to reproduce the structure and the vibrational spectra of kaolinite was tested in MD simulations. The initial framework structure is based on the data given by Young and Hewat[2] for a unit cell of *P*1 symmetry with the unit cell compositions $Si_4Al_4O_{10}(OH)_8$ and $Si_4Al_4O_{10}(OD)_8$. The simulation box consisted of $3 \times 2 \times 1$ unit cells, i.e., in total, 204 atoms (Figure 1). The equations of motion were integrated with the velocity form of the Verlet algorithm[32] with time steps of 0.4 fs under periodic boundary conditions. Initial velocities of the particles were taken from the Maxwell−Boltzmann distribution at 300 K. During the first 50 000 time steps the velocities of the atoms were rescaled to the reference temperature and then the simulations were continued in the NVE ensemble. The coordinates and velocities of all atoms were stored every fifth step for the last 40 960 from the total of 100 960 time steps (40.38 ps). The relative deviation of the total energy from the initial value over the NVE run was less than 10^{-4}, revealing a good conservation of the total energy.

The infrared spectra were calculated from the MD run via Fourier transformation of the autocorrelation function of the total dipole moment.[33] The effective atomic charges were set to the half of the values of the Mulliken 6-21G values computed by Hess and Saunders in a periodic Hartree−Fock calculation of kaolinite,[34] i.e., 1.25 e for Si, 1.05 e for Al, −0.85 e for O, and 0.28 e for H atoms.

Raman spectra in the region of the clay framework vibrations reveal a higher sensitivity to the structural characteristics than IR spectra, which show a quite similar pattern for different kaolinite polymorphs. Therefore, the Raman spectrum was examined in more detail. Raman spectra were calculated by Fourier transformation of the autocorrelation function of the polarizability tensor in an assumption that the polarizability of the system can be computed as a sum of bond polarizabilities.[35] The change of the system polarizability dP is then given by

$$\mathrm{d}P = \sum_i T_i^{-1}\, \mathrm{d}\alpha_i T_i \qquad (3)$$

where $\mathrm{d}\alpha_i$ and T_i denote the variation of the bond polarizability tensor and the matrix of direction cosines of the bond i, respectively. Within this approximation the Raman intensities were calculated, assuming that the equations developed for the Raman spectra of liquids are also valid for microcrystalline powders. The variation of the bond polarizability $\mathrm{d}\alpha_i$ was calculated following the electrooptical approach applied by Abbate et al.[36] for organic polymers. In the present work $\mathrm{d}\alpha_i$ was evaluated using only the derivatives of the longitudinal and transversal components of the bond polarizability with respect to the bond length. The variation of the longitudinal bond polarizability, $\delta\alpha_i^{\mathrm{L}}/\delta r_i$, was set to 2.27 Å^2 as previously derived for Si−O bonds from experimental band intensities in the vibrational spectra of the hydrosilasesquioxane $H_8Si_8O_{12}$.[37] A value of 0.64 Å^2 was employed[37] for the derivatives of the transversal components of the polarizability tensor, $\delta\alpha_i^{\mathrm{T}}/\delta r_i$. The same numeric values were assumed for the electrooptical parameters of the Al−O bonds. For O−H bonds the parameters were transferred from works on C−H bonds of hydrocarbons[36] because carbon is the next atom to oxygen in the periodic table for which electrooptical parameters have been determined. In test calculations it turned out that the relative intensities in the region of the framework vibrations are not very sensitive to variations of these parameters, which mostly influence intensities of the OH stretching modes not studied in detail in the present paper. In a first model used for calculation of the Raman spectra, only the longitudinal term was considered. In a second model, the complete form of the polarizability tensor was used to compute the variations of bond polarizabilities.

To get a better insight into participation of atoms of different types in the normal modes, the power spectra of the whole system, atoms of different types, and the primary building units of the structure were calculated. The spectra were computed by Fourier transformation of the velocity autocorrelation functions. In all calculated spectra the length of the used trajectory lead to a frequency step 8.14 cm^{-1}.

3. Results and Discussion

3.1. Force Field Development. As the force field for the silicate building units has already been described in detail elsewhere[21,22] we can focus here on changes and additional terms needed for kaolinite. The quantum mechanical calculations performed at the HF and MP2 levels for the $Al(OH)_6^{3-}$ model revealed C_1 as the point group for the energy minimum structure. The optimized bond lengths were calculated as 1.95 Å (HF/3-21 G*), 1.99 Å (HF/6-311 G**), and 2.01 Å (MP2/6-311 G**) for the Al−O bonds and as 0.975 Å (HF/3-21 G*), 0.95 Å (HF/6-311 G**), and 0.97 Å (MP2/6-311 G**) for the O−H bonds, respectively. The O−Al−O bond angles were optimized at 94° and 85° for HF/3-21 G*, 93.5° and 86.5° for HF/6-311 G**, and 95° and 85° for the MP2/6-311 G** calculation.

After transformation of the $\mathbf{F}_X$ matrix into the $\mathbf{F}_R$ matrix, the resulting force constants were used without any scaling procedure to extract the supplementary parameters of the force field necessary for kaolinite. The AlO stretching force constants obtained for the AlO_6 units at different levels of theory follow very closely the Badger's relation between the T−O stretching force constant and T−O bond length outlined for SiO_4 and AlO_4 tetrahedra in aluminosilicates.[22] According to this relationship, values of 1.26 and 1.7 mdyn/Å were derived for Al−O bonds in Al−O(Si)−O chains and Al−O(H)−O chains, respectively. These values correspond to AlO bond lengths of 2.01 and 1.86−1.90 Å obtained in the MP2 and HF/3-21G* calculations. For the bending force constants of nonlinear O−Al−O angles a value of 0.7 mdyn Å/rad^2 was derived by averaging the corresponding force constants of the MP2 calculation.

The cross-terms with the dominant numeric values were the same for the different levels of theory and basis sets adopted. Two different AlO/AlO interaction force constants can be distinguished in the AlO_6 octahedra. The first one corresponds to bonds, which are nearly perpendicular; they are not mechanically coupled and the corresponding cross-terms were therefore omitted. The second one is due to a nearly linear arrangement of AlO bonds with a common Al atom; the corresponding parameters are very small in all quantum mechanical calculations (smaller than 0.007 mdyn/Å in the MP2 calculation). Although these interaction force constants have significant Jacobian elements in the NMA calculations, the small value of the force constant leads to a negligible influence on the vibrational frequencies and the force constants were set to 0.0 mdyn/Å. After averaging the values for the AlO/OAlO and OAlO/OAlO force constants, the corresponding digits were very close to those obtained for AlO_4 tetrahedra.[22]

The force constants for Al−O(Si)−Al and Al−O(H)−Al chains were transferred from the aluminosilicate force field because the force constants of TOT bridges are known to be only weakly dependent on the nature of the T atoms.[22] The values for the AlOH bending and for OH/AlOH as well as AlOH/AlOH cross-terms for the protonated bridge were slightly reduced in order to reproduce the in-plane bending modes in the normal coordinate analyses. The OH stretching force

TABLE 1: Force Field Parameters for AlO_6 Octahedra and Al−O−Al Linkages Used in MD and NMA Calculations

internal coordinate	AlO_6 octahedron[a]
O−Al−O	0.70 (90°)
(AlO)/(AlO)	0.00
(OAlO)/(OAlO)[b]	−0.08
(OAlO)/(OAlO)[c]	−0.25
(AlO)/(OAlO)[b]	0.08
(AlO)/(OAlO)[c]	−0.08

internal coordinate	Al-O(H)−Al linkage	Al−O(Si)−Al linkage
Al−O	1.70 (1.86 Å)	1.26 (2.01 Å)
O−H	7.45 (1.00 Å)	
Al−O−H	0.16 (120°)	
Al−O−Al	0.14 (1.07°)	0.14 (95°)
(AlO)/(AlO)	0.17	0.00
(AlO)/(OH)	0.22	
(AlOH)/(AlOH)	−0.10	
(AlOH)/(AlOAl)	−0.06	
(AlOSi)/(AlOSi)		−0.09
(AlO)/(AlOH)[b]	0.00	
(AlO)/(AlOH)[c]	−0.10	
(OH)/(AlOH)	0.10	
(OH)/(AlOAl)	−0.17	
out-of-plane OH bending	0.00 (0°)	

[a] For AlO stretching force constant see the corresponding entry in the Al−O−Al linkages. [b] Entry refers to interaction force constant between internal coordinates with a common bond. [c] Entry refers to interaction force constant between internal coordinates with a common atom.

constant was set equal to 7.45 mdyn/Å in accordance with previous MD studies.[38]

The force field for the remaining structure units was directly transferred from the aluminosilicates work. Only the SiO stretching force constants in the SiO_4 units were readjusted using the parameters of the Badger's rule determined in ref 22 and the averaged experimental Si−O bond length[2] of 1.69 Å, yielding a force constant of 4.8 mdyn/Å for all Si−O bonds. The use of this bond length is not completely consistent with the equilibrium value, 1.64 Å, used in the calculation but leads to a better agreement between observed and calculated frequencies in the region of the SiO stretching modes. All the force field parameters for the Al-containing units are summarized in Table 1.

3.2. Molecular Dynamics Tests. As already mentioned by Hess and Saunders[34] the distribution of the internuclear distances in the work of Young and Hewat[2] is very wide (1.79−1.43 Å for Si−O and 2.06−1.66 Å for Al−O bonds). Such values are surprising from a chemical point of view, difficult to understand on the basis of the crystallographic structure. Such extreme bond lengths would lead to unrealistic stretching force constants and forces. To smooth out such structural features, a relatively long equilibration phase of 20 ps was chosen in the MD runs. As a result, after relaxation of the structure a narrow peak at 1.64 Å is obtained for the bond distance in the Si−O radial distribution function (RDF) depicted in Figure 2. This Si−O bond length agrees well with the value of 1.63 Å computed in MD simulations of kaolinite by Teppen et al.[19] The peaks at larger distances representing higher coordination spheres are more diffuse due to the low symmetry of the layer and to the large amplitude of the oxygen atoms motions. The Al−O RDF is visualized in Figure 3. Two distinct maxima are observed for the Al−O bond lengths at 1.91 and 2.05 Å with an intensity ratio of approximately 2:1. This ratio gives an estimation of the surface ratio of the two peaks and is in line with the results of neutron powder diffraction measurements of Bish[4] who determined considerably shorter bond lengths for the four

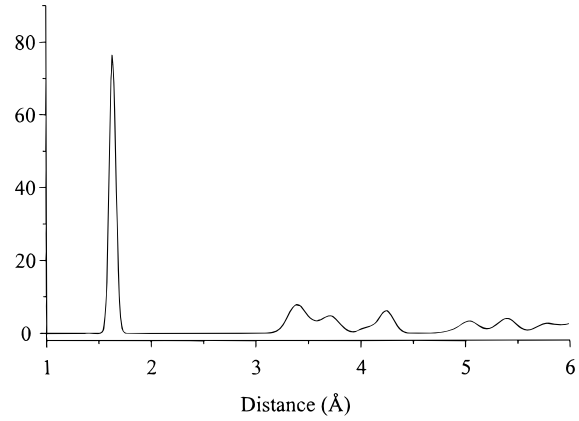

Figure 2. Calculated Si−O radial distribution function for kaolinite.

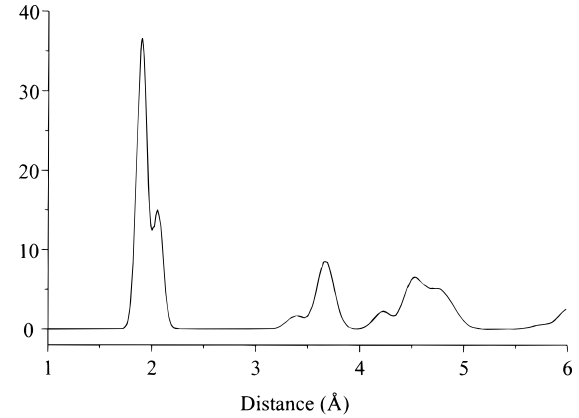

Figure 3. Calculated Al−O radial distribution function for kaolinite.

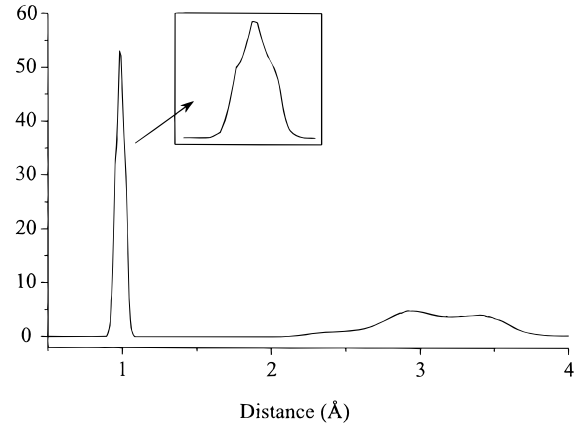

Figure 4. Calculated O−H radial distribution function for kaolinite.

protonated Al−O bonds in comparison with the two nonprotonated Al−O bonds within the AlO_6 octahedra. The second coordination sphere starts with peaks at 3.4 and 3.65 Å originating from the next oxygen atoms inside the sheet of AlO_6 octahedra and is followed by peaks at 4.2, 4.5, and 4.75 Å. In the O−H RDF (Figure 4) a strong peak with a maximum between 0.97 and 0.99 Å is obtained. It should be noted that the peak has several shoulders and is not really symmetric, as illustrated in the inset of Figure 4. This clearly indicates the heterogeneity of the OH groups expected in a crystal with *P*1 symmetry. However, a definite distinction in bond lengths between outer and inner OH groups could not be observed because only one set of parameters was used for all O−H bonds. The second and third peaks are found at 2.9 and 3.4 Å, in very close agreement with the nonbonded distances predicted for the

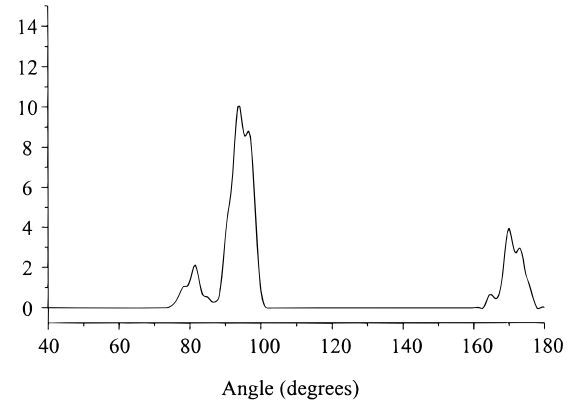

Figure 5. Calculated distribution function for O−Al−O angles in kaolinite.

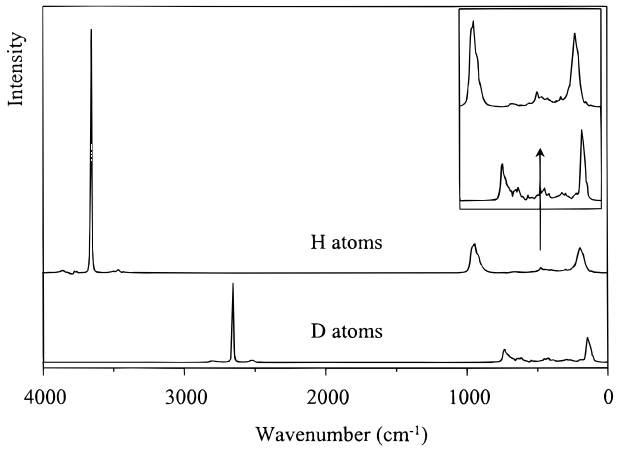

Figure 6. Calculated power spectra of the hydrogen and deuterium atoms.

hydrogen atoms of inner OH groups by periodic Hartree−Fock calculations of kaolinite.[34]

Figure 5 shows the calculated O−Al−O angle distribution function and reveals a blurred picture with maxima around 80° and in the ranges 90−97° and 170−178°. Whereas angles of around 90 and 180° could be expected for AlO_6 octahedra, O−Al−O angles around 80° are rather surprising. A closer inspection of the structure, however, shows that all angles smaller than 86° are found within the four-membered aluminate rings and lead to similar deviations of the linear angles. The ab initio calculations performed by Teppen et al.[20] for the neutral ring $Al(OH)_2(H_2O)_2-(OH)_2-Al(OH)_2(H_2O)_2$ molecular model revealed a comparable situation with smaller O−Al−O angles of about 82−85° (depending on the theory level) in the four-membered rings. In summary, the extended force field yields realistic structural characteristics and was successful in reproducing the structure of one kaolinite layer close to experimental data.

In the discussion of the vibrational spectra we first will focus on the normal modes of the OH groups, which can be identified in the power spectra of the hydrogen and deuterium atoms shown in Figure 6. The band of the OH stretching mode is shifted upon deuteration from 3656 to 2655 cm^{-1}. The calculated shift of $\Delta\tilde{\nu} = 1001$ cm^{-1} is very close to the observed shift in the infrared spectra of $\Delta\tilde{\nu} = 972-953$ cm^{-1}.[6] The OH(D) in-plane bending modes can, in agreement with data from the literature,[10,11] unambiguously be assigned to bands at 940 and 730 cm^{-1}, respectively. The calculated shift of $\Delta\tilde{\nu} = 210$ cm^{-1} upon the isotopic substitution is again in good agreement with the experimental observations of $\Delta\tilde{\nu} = 220$ cm^{-1}.[10] Only for

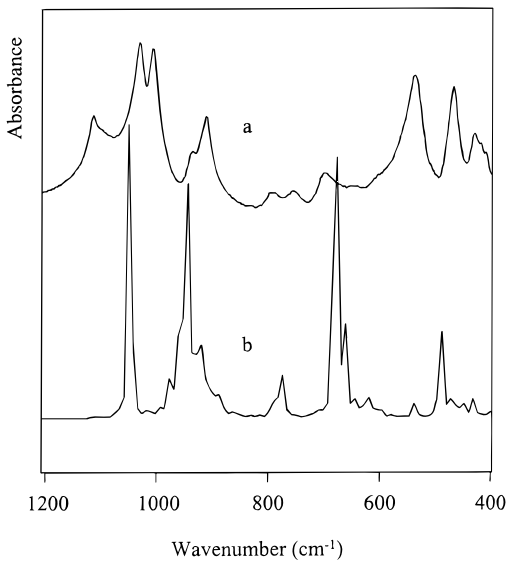

Figure 7. Experimental (a) and calculated (b) infrared spectrum of kaolinite in the framework region. The experimental spectrum was taken from the kaolinor sample.

the OH out-of-plane bendings must a discrepancy with empirical assignments be outlined. Whereas in the experimental infrared spectra these modes were attributed to bands at 405 and below 300 cm^{-1},[10] the calculations revealed bands at 195 and 145 cm^{-1} for the OH(D) out-of-plane bendings. This disagreement may easily be explained by a small value of the force constant of 0.03 (mdyn Å)/rad^2, which is close to the precision limit of the computational procedure used but is in good correlation with the fact that the Al−O bonds in $O_5Al\cdots OH\cdots AlO_5$ linkages are very weak. Far-infrared spectra of deuterated clay samples would be useful but are presently not available in the literature and are extremely difficult to obtain in a sufficient quality to draw definitive conclusion on this issue.

In the OH stretching range of the IR spectrum instead of four bands at 3696, 3669, 3653, and 3620 cm^{-1} in the experiment only a single sharp band at 3656 cm^{-1} with a small shoulder at 3668 cm^{-1} was obtained in the calculation. The single peak in the OH stretching range is not surprising because one force constant was used for all OH groups and long-range electrostatic interactions, which could lead to band splittings, were not explicitly considered in the force field. The absence of splitting in the simulated OH band excludes the existence of mechanical coupling between modes of different OH groups leading to in-phase or out-of-phase modes often assumed in empirical assignments of kaolinite spectra.[6] This result suggests that the observed splitting can be caused by long-range through-space interactions probably of electrostatic nature.

The experimental and calculated IR spectra in the framework region are depicted in Figure 7. Even if the intensities of the experimental IR spectrum are not well reproduced over the whole spectral range, each observed band has its counterpart in the computed spectrum (see also Table 2). The experimental Raman spectra of the kaolinor and granulite samples are presented in Figure 8 together with the spectra computed from the MD trajectory using different sets of electrooptical parameters and normalized to the most intense Raman line at about 500 cm^{-1}. The Raman spectra recorded from powders correspond to the scattering of crystallites averaged over all orientations and modified by multiple and diffuse reflection. So the spectra are dependent on the size and the nature of the particles, and according to the different nature of the two samples, it is not surprising that the Raman spectra of kaolinor

TABLE 2: Observed and Calculated Vibrational Frequencies (cm^{-1}) of Kaolinite and Proposed Assignment

infrared		Raman		
exp	comp	exp	comp	proposed assignment
3696				OH stretch
3669	3668			OH stretch
3653	3656		3656	OH stretch
3620				OH stretch
1115		1112	1051	SiO stretch (TOT)
1031	1050			SiO stretch (TOT)
1007				SiO stretch (TOT)
937	945		944	OH bend + framework
912	920	913	912	OH bend + framework
796				Si translation
789	788	790	790	Si translation
755	774	751	773	SiO stretch
697	675	707	709	SiO stretch
643	659			AlO stretch
537	538	509	538	OSiO bend + TO stretch
		475	472	OTO bend + TO stretch
468	488	464	456	OTO bend + TO stretch
430	430	430	432	OTO bend (OAlO)
		337	302	bend
270[a]	260	271	260	bend
244[a]		246	244	bend
205[a]	203	196	188,171	bend, OH bend (?)
		143[b]	138	bend
		120[b]		bend

[a] Reference 14. [b] Reference 9.

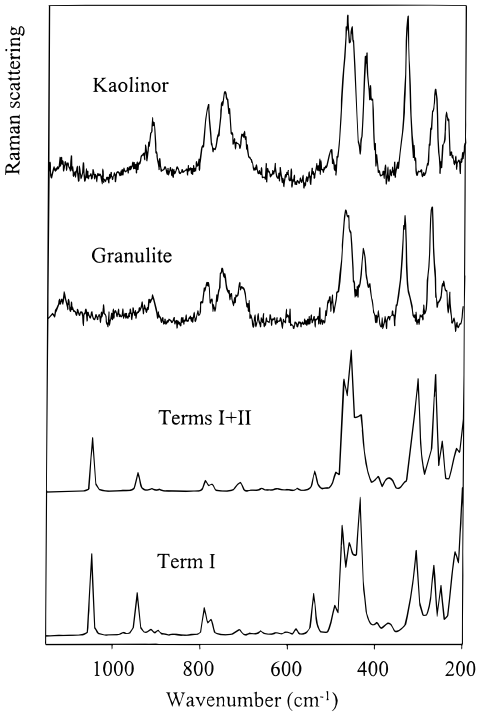

Figure 8. Raman spectra of the kaolinite samples kaolinor and granulite in comparison with the spectra simulated using electrooptical parameters.

and granulite differ mostly in the intensities of several lines. The kaolinor sample obtained after separation of most of the quartz and mica components and drying processes is therefore the most suitable sample for comparison with the spectra calculated from the MD runs. There is a good overall agreement between the observed and calculated spectra (Figure 8); especially in the simulation taking longitudinal and transversal electrooptical parameters into account, a substantial improvement was achieved. The consideration of the transversal bond polarizability derivatives leads to an intensity decrease for the

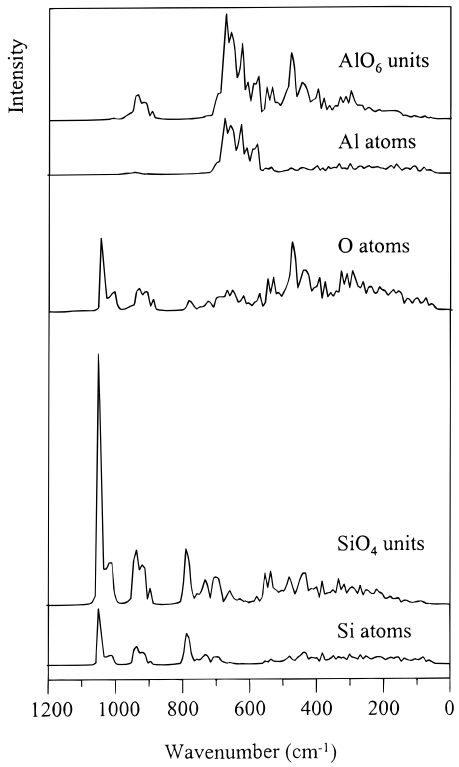

Figure 9. Calculated power spectra of silicon, oxygen, and aluminum atoms in comparison with the power spectra of SiO_4 and AlO_6 primary building units.

Raman lines above 750 cm^{-1} and to an increase for the bands below 350 cm^{-1} in good agreement with the experimental data. A correlation coefficient of 0.998 between the calculated and experimental positions of the bands in the vibrational spectra was obtained for the frequency region below 1200 cm^{-1}.

To obtain a more reliable assignment of the observed bands to specific modes, the calculated IR and Raman spectra should be discussed in connection with the power spectra computed for each kinds of atom and for the primary building units. The spectra of the silicon, oxygen, and aluminum atoms as well as the SiO_4 and AlO_6 primary building units are collected in Figure 9 and the derived assignments of the IR and Raman spectra are summarized in Table 2.

In the range 1120−1000 cm^{-1} the calculated IR spectrum shows only a single band at 1050 cm^{-1}, whereas in the experiment the absorption is clearly split into a doublet with maxima at 1031 and 1007 cm^{-1} and an additional band at 1115 cm^{-1}. This relatively large number of bands in the experimental spectrum might be attributed to deviations of the SiO six-membered rings from hexagonal symmetry in the kaolinite sample. The absence of the high-frequency shoulder at 1115 cm^{-1} in the simulated spectrum can be caused by the simplification in the present potential model where the same SiO force constant was applied for SiOSi and SiOAl bridges. Bands in this frequency region correspond to asymmetric modes of TOT bridges, and it was shown for siliceous zeolites that the frequencies of these modes are dependent on SiO force constants of the TOT bridge.[39] In the power spectra of silicon atoms, oxygen atoms, and SiO_4 units in Figure 9 a sharp maximum at 1050 cm^{-1} with a shoulder at 1011 cm^{-1} is clearly visible. Therefore, these bands have to be assigned to SiO stretching modes. The band positions are in close agreement with the observed bands in the infrared spectra at 1031 and 1007 cm^{-1}. The proposed assignment may further be assisted by calculations of the Raman spectra taking solely the electrooptical parameters

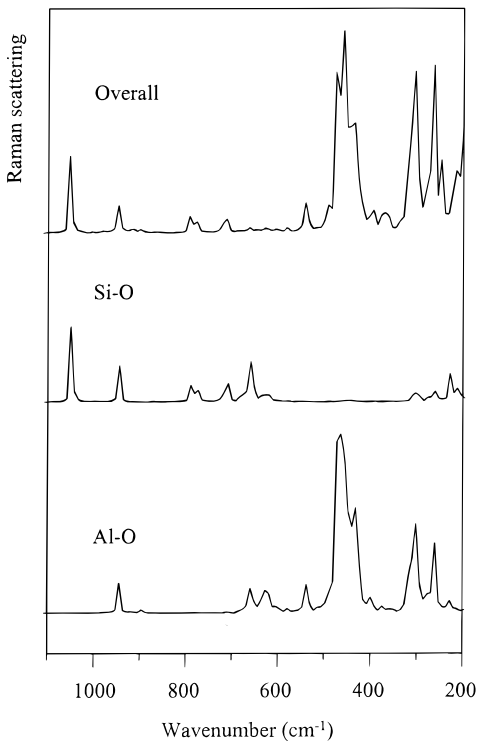

Figure 10. Simulated Raman spectra of kaolinite taking into account solely the electrooptical parameters for the Si−O bonds and the Al−O bonds and overall spectrum, respectively.

for the Si−O bonds or solely for the Al−O bonds into account. In this way the contributions of both parts to the overall Raman spectrum can be separated. The calculated spectra are shown in Figure 10 and confirm the derived assignment in the spectral range 1120−1000 cm^{-1}.

In the region around 950 cm^{-1} the dominant absorption has already been assigned to OH in-plane bending modes. Nevertheless, it should be noted that peaks at 935 and 930 cm^{-1} are observed especially in the power spectra of AlO_6 and SiO_4 primary building units. So the peak at 935 cm^{-1} should be interpreted by taking into account a significant interaction between TO stretching coordinates and the OH in-plane bending coordinate (δOH). A corresponding large coupling appeared in the NMA as a large Jacobian matrix element for the AlO/δOH interaction force constant. The proposed assignment accounts for a relatively low value of $\delta OH/\delta OD = 1.29$ upon deuteration.

Below 1000 cm^{-1} the power spectrum of the oxygen atoms (Figure 9) indicates that the oxygen atoms are involved in most of the normal modes. It is worthy to note that in the spectral range between 900 and 775 cm^{-1} the power spectrum of the oxygen atoms has no significant intensity, in opposition to the spectra of silicon atoms and SiO_4 primary building units, which show peaks at 790 cm^{-1}. This can be interpreted in terms of nearly isolated displacements of the silicon atoms (Si translation). This assignment is corroborated by the fact that ^{17}O and ^{18}O isotope substitution in siliceous zeolites leads to red shifts of nearly all bands in the experimental infrared spectra, except the band at 800 cm^{-1}.[40] In the Raman spectrum three lines were observed in this region at 790, 751, and 707 cm^{-1}; they are nicely reproduced in the simulation. The latter two were attributed to SiO stretching modes.

In the region below 700 cm^{-1} the power spectrum of aluminum atoms shows a broad maximum between 670 and 580 cm^{-1} whereas the spectrum of AlO_6 units is well structured with dominant maxima at 670, 625, 481, and 302 cm^{-1}. With the exception of the above-mentioned peak at 935 cm^{-1} the power spectra of the aluminum atoms and the AlO_6 units do not show vibrations in the range above 700 cm^{-1}. This leads, in accordance to our NMA results, to the conclusion that AlO modes are concentrated below 670 cm^{-1}. This result is in line with the conviction deduced from numerous experimental data that AlO stretching frequencies of AlO_6 octahedra in silicates are in any case not appreciably higher than 650−600 cm^{-1}.[10] The calculated peaks at 670 and 625 cm^{-1} must then originate from AlO stretching modes detectable in the IR spectra by a weak absorption at 643 cm^{-1}. In the calculated Raman spectra the two modes are reflected only in the AlO part by two lines at 650 and 630 cm^{-1} and in the SiO part at 661 cm^{-1} (Figure 10).

In the following region between 540 and 450 cm^{-1} the Raman spectrum is characterized by a weak line at 511 cm^{-1} and by a very strong doublet at 475 and 464 cm^{-1}, which is very well reproduced in the calculated spectra. Whereas the weak band at 511 cm^{-1} can easily be assigned to OSiO bending modes by the criterion of appreciable amounts in the SiO_4 power spectrum and the absence in that of the silicon atoms, the nature of the dominant doublet seems to be more complex. It is interesting to note that a similar doublet is observed in the Raman spectra of dealuminated faujasites and it is sensitive to the aluminum content at low levels.[41] However, the origin of this splitting is still under discussion in the case of zeolites. For kaolinite structure, the power spectrum of oxygen atoms shows a strong maximum at this position. Peaks around 475 cm^{-1} can clearly be identified in the spectra of the SiO_4 and AlO_6 units. However, these peaks are absent in the power spectrum of the *T* atoms. One possible explanation is that, in analogy to SiO_2 polymorphs,[42] the motion may be interpreted as a motion of the bridging oxygen atoms in the plane bisecting the TOT bridges involving OTO bending and TO stretching degrees of freedom. The intense Raman line at 430 cm^{-1} corresponds to similar motions with dominant AlO contributions.

Below 400 cm^{-1} the developed force field is well suited to reproduce the experimental Raman spectrum with a high accuracy. The comparison of different contributions reveals complex couplings of motions in this frequency range. Following our NMA results these modes belong to bendings including a high degree of coupling between OTO and TOT angle deformations.

4. Conclusions

In this paper the vibrational spectra and structure of kaolinite have been investigated by the concomitant use of IR and Raman spectroscopies complemented by quantum mechanical calculations, normal-mode analyses, and MD simulations. Parameters of the generalized valence force field for 6-fold coordinated aluminum atoms were derived by ab initio quantum chemical calculations and combined with the force field for tetracoordinated Si and Al atoms in aluminosilicates.[21,22] The resulting clay force field was applied for NMA and MD simulations and yields a structure and vibrational spectra of the mineral in close agreement with the experimental data. From the comparison of experimental IR and Raman spectra with the results of calculations, an assignment of the experimental data is proposed. The best overall correspondence with the experimentally observed Raman spectrum was achieved by computing Raman intensities with a three-parameter approach in the frames of the valence optical theory. The calculated Raman intensities indicate the validity and transferability of the set of electrooptical parameters previously determined for aluminosilicates.

The results of the present work confirm that the joint application of experimental and theoretical methods is a valuable tool for exploring the structure and dynamics of complex structures. The force field developed is expected to be helpful in predictions and in interpretation of the vibrational spectra of other clay minerals. The results can further be used in modeling studies of intercalated species, where the high flexibility of the clay sheets due to the low-frequency motions can interfere with the dynamics of guest species.

Acknowledgment. E.G. gratefully acknowledges the financial support for a research fellowship from the "Centre National de la Recherche Scientifique". This report is part of the "Programme de Recherche Concerté: Sites et Sols Pollués" supported by the Région Nord/Pas de Calais and the Fonds Européen de Développement Economique des Régions (FEDER). The authors thank Dr. B. Sombret and Dr. J. Laureyns for recording the experimental infrared and Raman spectra.

References and Notes

(1) Pauling, L. *Proc. Natl. Acad. Sci. U.S.A.* **1930**, *16*, 578.
(2) Young, R. A.; Hewat, A. W. *Clays Clay Miner.* **1988**, *36*, 225.
(3) Bish, D. L.; Von Dreele, R. B. *Clays Clay Miner.* **1989**, *37*, 289.
(4) Bish, D. L. *Clays Clay Miner.* **1993**, *41*, 738.
(5) Hobbs, J. D.; Cygan, R. T.; Nagy, K. L.; Schultz, P. A.; Sears, M. P. *Am. Mineral.* **1997**, *82*, 657.
(6) Rouxhet, P. G.; Samudacheata, N.; Jacobs, H.; Anton, O. *Clay Miner.* **1977**, *12*, 171.
(7) Johnston, C. T.; Agnew, S. F.; Bish, D. L. *Clays Clay Miner.* **1990**, *38*, 573.
(8) Pajcini, V.; Dhamelincourt, P. *Appl. Spectrosc.* **1994**, *48*, 638.
(9) Frost, R. L. *Clay Miner.* **1997**, *32*, 65.
(10) Lazarev A. N. *Vibrational Spectra and Structure of Silicates*; Consultants Bureau: New York, 1972.
(11) Frost, R. L. *Clays Clay Miner.* **1998**, *46*, 280.
(12) Ledoux, R. L.; White, J. L. *Science* **1964**, *145*, 47.
(13) Wada, K. *Clay Miner.* **1967**, *7*, 51.
(14) Frost, R. L.; Fredericks, P. M.; Bartlett, J. R. *Spectrochim. Acta* **1993**, *49A*, 667.
(15) Frost, R. L.; Tran, T. H.; Kristof, J. *Vibr. Spectrosc.* **1997**, *13*, 175.
(16) Frost, R. L.; Tran, T. H.; Rintoul, L.; Kristof, J. *Analyst* **1998**, *123*, 611.
(17) Frost, R. L.; Kristof, J.; Paroz, G. N.; Kloprogge, J. T. *J. Phys. Chem. B* **1998**, *102*, 8519.
(18) Teppen, B. J.; Rasmussen, K.; Bertsch, P. M.; Miller, D. M.; Schäfer, L. *J. Phys. Chem. B* **1997**, *101*, 1579.
(19) Teppen, B. J.; Yu, C.-H.; Newton, S. Q.; Miller, D. M.; Schäfer, L. *J. Mol. Struct.* **1998**, *445*, 65.
(20) Smirnov, K. S.; Bougeard, D. *J. Phys. Chem.* **1993**, *97*, 9434.
(21) Ermoshin, V. A.; Smirnov, K. S.; Bougeard, D. *Chem. Phys.* **1996**, *202*, 53.
(22) Ermoshin, V. A.; Smirnov, K. S.; Bougeard, D. *Chem. Phys.* **1996**, *209*, 41.
(23) Ermoshin, V. A.; Smirnov, K. S.; Bougeard, D. *Surf. Sci.* **1996**, *368*, 147.
(24) Loh, E. *J. Phys. C: Solid State Phys.* **1973**, *6*, 1091.
(25) Bärtsch, M.; Bornhauser, P.; Calzaferri, G.; Imhof, R. *J. Phys. Chem.* **1994**, *98*, 2817.
(26) Hill, J.-R.; Sauer, J. *J. Phys. Chem.* **1995**, *99*, 9536.
(27) Frisch, M. J.; Trucks, G. W.; Schlegel, H. B.; Gill, P. M. W.; Johnson, B. G.; Robb, M. A.; Cheeseman, J. R.; Keith, T.; Petersson, G. A.; Montgomery, J. A.; Raghavachari, K.; Al-Laham, M. A.; Zakrzewski, V. G.; Ortiz, J. V.; Foresman, J. B.; Cioslowski, J.; Stefanov, B. B.; Nanayakkara, A.; Challacombe, M.; Peng, C. Y.; Ayala, P. Y.; Chen, W.; Wong, M. W.; Andres, J. L.; Replogle, E. S.; Gomperts, R.; Martin, R. L.; Fox, D. J.; Binkley, J. S.; Defrees, D. J.; Baker, J.; Stewart, J. P.; Head-Gordon, M.; Gonzalez C.; Pople, J. A. *Gaussian 94*, Revision C.2; Gaussian Inc.: Pittsburgh, PA, 1995.
(28) Teppen, B. J.; Miller, D. M.; Newton, S. Q.; Schäfer, L. *J. Phys. Chem.* **1994**, *98*, 12545.
(29) Allouche, A.; Pourcin, J. *Spectrochim. Acta* **1993**, *49A*, 571. Allouche, A. *Redong*, QCPE 628.
(30) Jones, R. N. *Computer Programs for Infrared Spectrophotometry—Normal Coordinate Analyses*; NRCC Bulletin No 15; NRCC: Ottawa, Canada, 1976.
(31) Shimanouchi, T. *Computer Programs for Normal Coordinate Treatment of Polyatomic Molecules*; University of Tokyo, 1968.
(32) Swope, W. C.; Anderson, H. C.; Berens, P. H.; Wilson, K. R. *J. Chem. Phys.* **1982**, *76*, 637.
(33) Berens, P. H.; Wilson, K. R. *J. Chem. Phys.* **1981**, *74*, 4872.
(34) Hess, A. C.; Saunders, V. R. *J. Phys. Chem.* **1992**, *96*, 4367.
(35) Smirnov, K. S.; Bougeard, D. *J. Raman Spectrosc.* **1993**, *24*, 255.
(36) Abbate, S.; Gussoni, M.; Masetti, G.; Zerbi, G. *J. Chem. Phys.* **1977**, *67*, 1519.
(37) Bornhauser, P.; Bougeard, D. Proceedings of the 9th Deutsche Zeolithtagung, Halle, 1997.
(38) Koudriachova, M.; Geidel, E. In *Proceedings of the 12th International Zeolite Conference*, Baltimore, 1998; Treacy, M. M. J., Marcus, B., Higgins, J. B., Bisher, M. E., Eds.; Materials Research Society: Warrendale, PA, 1998; I, p 423.
(39) Geidel, E.; Bauer, F.; Böhlig, H.; Kudra, M. *Acta Chim. Hung.—Models Chem.* **1995**, *132*, 349.
(40) Bauer, F.; Geidel, E.; Peuker, C.; Pilz, W. *Zeolites* **1996**, *17*, 278.
(41) Brémard, C.; Le Maire, M. *J. Phys. Chem.* **1993**, *97*, 9695.
(42) McMillan, P. F. *Am. Mineral.* **1984**, *69*, 622.